

## Thermalization of electron-hole pairs in LaBr<sub>3</sub>, CeBr<sub>3</sub> and CLLB: Monte Carlo simulation

Fei Gao<sup>1,\*</sup>, Zhe Shi<sup>2,3</sup>, Ju Li<sup>2,3</sup> and Jarek Glodo<sup>4</sup>

<sup>1</sup>Department of Nuclear Engineering and Radiological Science, University of Michigan, Ann Arbor, Michigan 48109-2104, USA

<sup>2</sup>Department of Nuclear Science and Engineering, Massachusetts Institute of Technology, Cambridge, Massachusetts 02139-4307, USA

<sup>3</sup>Department of Materials Science and Engineering, Massachusetts Institute of Technology, Cambridge, Massachusetts 02139-4307, USA

<sup>4</sup>Radiation Monitoring Devices, Inc., Watertown, Massachusetts 02472-4624, USA



(Received 1 August 2023; accepted 5 January 2024; published 5 February 2024)

A Monte Carlo model is used to investigate electron-hole ( $e-h$ ) generation created by incident gamma-ray radiation in LaBr<sub>3</sub>, CeBr<sub>3</sub>, and Cs<sub>2</sub>LiLaBr<sub>6</sub> (CLLB) scintillators. Our approach follows the detailed energy loss mechanisms and describes the microscopic structure of ionization tracks in order to address differences in the scintillation properties of these three materials. The mean energy required to create an  $e-h$  pair,  $W$ , theoretical light yield, and the spatial distribution of  $e-h$  pairs are determined. We found that  $W$  approaches constant and similar values at high incident energies for LaBr<sub>3</sub> and CLLB, suggesting that these materials should have similar light yields. However, the experimental light yield of CLLB is almost half that of LaBr<sub>3</sub>. Unlike for LaBr<sub>3</sub>,  $W$  of CeBr<sub>3</sub> increases with increasing energy excitation and shows a nonlinear behavior in  $e-h$  creation, potentially explaining slightly lower light yield and worse energy resolution of CeBr<sub>3</sub>. Furthermore, we observed that the spatial distributions of electron-hole pairs in LaBr<sub>3</sub> and CeBr<sub>3</sub> are very similar, while the number of high-density  $e-h$  domains in CLLB is greater in comparison. This discrepancy could explain the lower light yield of CLLB. The thermalization model of  $e-h$  pairs showed that the longitudinal optical phonon energy has a profound effect on the thermalization time and distance of  $e-h$  pairs, leading to a much higher density of excitation in LaBr<sub>3</sub> but a more diffuse one in CLLB. This effect leads to steeper gradients in LaBr<sub>3</sub>, resulting in varying density effects and worse proportionality, while CLLB suffers from more uniform but more pronounced quenching. The fraction of nonradiatively recombined electrons in LaBr<sub>3</sub> and CLLB was estimated to be 30% and 45%, respectively. These results correlate well with experimental observations of the scintillation properties of these materials. The approach can be used to predict the expected properties of new materials and support further development of existing materials.

DOI: [10.1103/PhysRevMaterials.8.025201](https://doi.org/10.1103/PhysRevMaterials.8.025201)

### I. INTRODUCTION

The generation of electron-hole ( $e-h$ ) pairs and their thermalization are fundamental processes that significantly affect light yield, light yield nonlinearity, and energy resolution in scintillation materials. The effects of nonlinearity can significantly deteriorate their achievable energy resolution in many cases limiting their utility. As a result, numerous efforts have been devoted to understanding the origins of scintillation processes that give rise to nonlinearity. Previously, several models have been proposed to investigate the light yield nonlinearity of inorganic scintillators. In an early model by Dorenbos *et al.* [1], the  $e-h$  pair tracks simulated using a radiation transport code were combined with an analytical function to describe the luminescence efficiency and model the nonlinearity in NaI (Tl). In addition, a phenomenological model proposed by Bizarri *et al.* [2–4] considered both radiative and nonradiative processes, but employed a linear, quadratic, or cubic dependence on  $e-h$  pair density. This model used the Bethe-Bloch equation or energy loss function to represent  $e-h$  pair density, whereas different energy transfer processes were described

using a series of analytical rate equations. Furthermore, Payne *et al.* [5] proposed a similar model by using linear densities obtained from the Bethe-Bloch equation, and concluded that the recombination of  $e-h$  pairs and exciton-exciton annihilation represents two competing processes corresponding to the generation of light yield in scintillator materials. Despite the simplicity, this model demonstrated that the nonlinearity response curves of a wide range of inorganic scintillators can be successfully fitted. One of the key factors in all these models is to assume that nonlinearity is ultimately correlated to the energy dependence of the density of  $e-h$  pairs along ionization tracks. Thus, the fundamental understanding of track structures created by the interaction of high-energy particles within inorganic scintillators is crucial for modeling the nonlinear response of these materials.

More recently, Williams *et al.* [6] developed a finite-element model with a Gaussian profile representing the  $e-h$  pair track to explore the role of carrier diffusion on carrier quenching and, consequently, on nonlinearity. Their results highlighted that diffusion, drift, Auger quenching, and dipole-dipole quenching are key processes affecting the survival of free charge carriers that need to escape the volume of high density to be trapped by luminescence centers and contribute to the emission of photons. To realize the role of carrier

\*Corresponding author: gaofei@umich.edu

quenching on nonlinearity, Wang *et al.* [7,8] developed a Monte Carlo electron thermalization model, which considers the effects of internal electric fields on the mobility of charge carriers and electron scattering with both longitudinal optical (LO) and acoustic phonons (LA/TA). The model used the  $e$ - $h$  pair spatial distributions generated by Northwest Electron and Gamma Ray Interaction with Matter (NWEGRIM) and was applied to the alkali halide (CsI and NaI) and the alkaline earth halide (CaF<sub>2</sub> and BaF<sub>2</sub>) materials. The thermalization simulations demonstrated that the LO phonon energy strongly affects the electron thermalization process: The smaller the LO phonon energy is, the longer the thermalization time and distance are.

In this work, we used the NWEGRIM code [9,10] to determine  $e$ - $h$  pair creation and their spatial distribution along ionization tracks in Ce<sup>3+</sup> doped LaB<sub>3</sub>, CeBr<sub>3</sub>, and Ce<sup>3+</sup> doped Cs<sub>2</sub>LiLaBr<sub>6</sub> (CLLB). We also extended the electron thermalization model to investigate the recombination of  $e$ - $h$  pairs at lattice sites and the survival of free charge carriers that escape from the volume of high ionization density to be captured by luminescence centers and recombine with desired emission of photons. LaB<sub>3</sub>:Ce and CeBr<sub>3</sub>, both with hexagonal crystal structures, are types of detector materials with their energy resolution (better than 3–4% at 662 keV) and light output (>60 000 ph/MeV) better than these for NaI:Tl (6% at 662 keV, 45 000 ph/MeV). These materials are good for  $\gamma$ -ray spectroscopy due to their excellent energy resolution and fast response [11,12]. CLLB belongs to the elpasolite crystal family with a cubic structure, and is a highly promising material for  $\gamma$ -ray spectroscopy and thermal neutron detection due to the Li component. CLLB also has a high light output (>40 000 ph/MeV), good energy resolution (<3.5% at 662 keV), and very good proportionality. It is the proportionality that sets it apart from the trihalides, which show nonlinear responses at lower energies of excitation. The cubic crystal structure of CLLB also gives it an advantage for the crystal growth, as having isotropic expansion coefficient reduces thermal stress resulting in crystal cracking and lower yields. While similar in some ways, they do differ in others, therefore we believe that a comparison of these materials may provide a pathway to identify the role of the thermalization process and carrier quenching on nonlinearity and energy resolution.

## II. MODELING APPROACHES

The scintillation process can be divided into three stages: (1) the electron cascade, that is, the production of electron-hole pairs following the absorption of an incident gamma-ray; (2) the hot electrons and holes undergoing thermalization to the bottom of the conduction band and the top of the valence band, respectively; and (3) the radiative emission of light either via the radiative decay of self-trapped excitons (STE) or through energy transfer to luminescence centers, which then relax radiatively. In the current study, we consider two stage mechanisms, i.e., electron-hole pair creation and their thermalization, to understand how the thermalization process affects the nonlinearity observed in scintillator materials. The thermalization process occurs much faster than the stage 3 one, and thus, the radiative process can be neglected during thermalization.

### A. $e$ - $h$ creation

To model the thermalization process, the spatial distribution of  $e$ - $h$  pairs generated by  $\gamma$ -ray excitation is first simulated through NWEGRIM, which includes a number of energy loss mechanisms for an incident photon and fast electrons. The interaction of an incident photon with an atom engages inner-shell photoionization, Compton scattering, or electron-positron pair production to create a high kinetic energy electron (also called delta rays), where their relative probability can be computed from the corresponding cross sections [13]. The fast electron can interact with an atom to further create  $e$ - $h$  pairs along its path, which occurs through various energy loss mechanisms, including valence to conduction interband transitions, plasmon excitations, core-shell ionizations, electron-phonon interactions, and Bremsstrahlung emission. The general algorithm of NWEGRIM has been detailed in our previous works [7,10]. Here, the NWEGRIM code is applied to LaB<sub>3</sub>, CeBr<sub>3</sub>, and CLLB to understand the creation of  $e$ - $h$  pairs and their track structures, which are used as inputs for the thermalization simulations. The 96 incident photon energies ranging from 50 eV to 662 keV are simulated to study the intrinsic scintillation properties of these materials, and 10<sup>5</sup> events are simulated for each photon energy to have good statistics on the number of  $e$ - $h$  pairs created and their number distribution to ensure convergence of the calculated values of  $W$  (work function). However, only six incident  $\gamma$ -ray energies of 2, 5, 10, 20, 100, and 400 keV are elected to carry out thermalization studies due to computational costs. The  $e$ - $h$  pair histories are further analyzed to yield the electron density along the tracks and the final kinetic energy distribution, which are also important inputs for thermalization simulation. A very large supercell can be used for the simulation without significantly increasing simulation time, and thus, the boundary conditions (the periodic boundary conditions are used in the current study) do not affect the simulation results.

### B. Thermalization process

A Monte Carlo algorithm used to model the thermalization process was previously developed [7,8], and has been applied to a number of scintillator materials. The thermalization model is detailed in our previous publications, and its general principle is briefly described here. In the model, several energy loss mechanisms are considered, including the interaction of electrons with longitudinal optical (LO) and acoustic ( $A$ ) phonons, i.e., LO phonon emission, LO phonon absorption,  $A$  phonon emission, and  $A$  phonon absorption. In addition, the internal electric field generated by the cloud of electrons and holes is also evaluated, and its influence on the electron trajectories is calculated using the classical equations of electrodynamics. Similar to the previous model, the electron kinetics is fully described, but the holes are assumed to be self-trapped instantaneously and immobile after the creation by a cascade. The electron-phonon interaction models formalized by Llacer and Garwin [14] and Sparks *et al.* [15] are used to determine the scattering rates, scattering angles, and inverse mean free paths for emission and absorption of LO and  $A$  phonons, respectively, where the correction by Bradford and Woolf [16] is also made for the electron- $A$  phonon

TABLE I. Primary model parameters for thermalization.

Parameters	Definition	LaBr <sub>3</sub>	CeBr <sub>3</sub>	CLLB
$a_0$ (nm)	lattice constant	0.795 <sup>a</sup>	0.795 <sup>b</sup>	1.141 <sup>c</sup> 1.049 <sup>d</sup>
$c_0$ (nm)	lattice constant	0.450	0.444	
Structure	lattice type	hexagonal <sup>a</sup>	hexagonal <sup>b</sup>	cubic <sup>d</sup>
	group	$P6_3/M^a$	$P6_3/M^b$	$Fm3m^d$
$\epsilon_\infty$	optical dielectric constant	4.91 <sup>a</sup>		3.155 <sup>c</sup>
$\epsilon_0$	static dielectric constant	10.0 <sup>a</sup>		14.14 <sup>c</sup>
$C_{11}$ (GPa)	elastic constant <sup>e</sup>	40.98 <sup>f</sup>	28.0 <sup>g</sup>	34.58 <sup>d</sup>
$C_{12}$ (GPa)	elastic constant	5.75 <sup>f</sup>	10.0 <sup>g</sup>	6.74 <sup>d</sup>
$C_{44}$ (GPa)	elastic constant	19.63 <sup>f</sup>	21.0 <sup>g</sup>	6.59 <sup>d</sup>
$\hbar\omega_{LO}$ (eV)	LO phonon energy	0.023 <sup>a</sup>		0.024 <sup>c</sup>
$\hbar\omega_{AO}$ (eV)	AO phonon energy	0.016 <sup>a</sup>		0.005 <sup>c</sup>
$m^*/m$	electron effective mass	1.32 <sup>h</sup>		4.92 <sup>c</sup>
$\eta$	electron affinity	0.3		1.706 <sup>c</sup>

<sup>a</sup>Reference [17].<sup>b</sup>Reference [20].<sup>c</sup>*Ab initio* calculations.<sup>d</sup>Reference [22].<sup>e</sup>The elastic constants of Cs<sub>2</sub>NaLaBr<sub>6</sub> are used because its electronic structure and composition are similar to those of Cs<sub>2</sub>LiLaBr<sub>6</sub>.<sup>f</sup>Reference [18].<sup>g</sup>Reference [21].<sup>h</sup>Reference [19].

interactions. In order to determine the electron-phonon interactions, the model parameters need to be determined and used for thermalization simulations. As described in [8], there are two-class parameters, i.e., the first class that is determined from experimental data or *ab initio* calculations and the second class that is calculated from the first-class parameters. The formulations used to obtain the second-class parameters are discussed in detail in [8], and here the first-class parameters are listed in Table I, along with their sources.

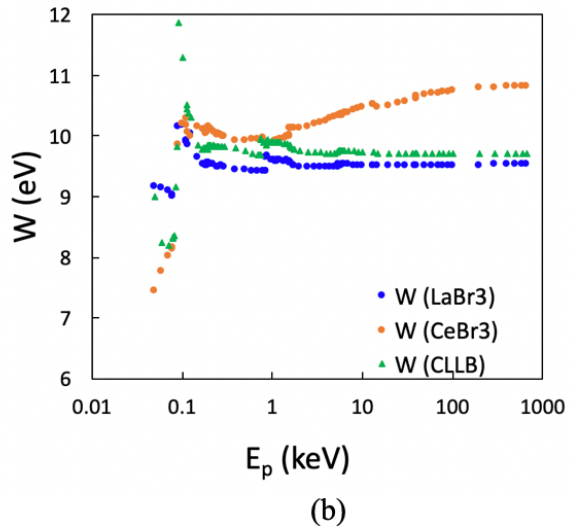
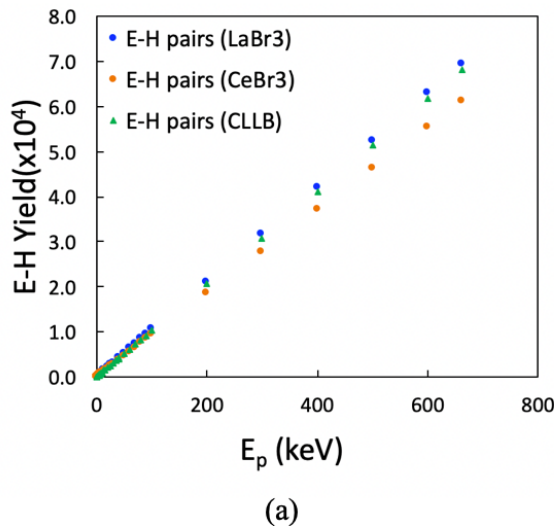


FIG. 1. Simulated electron-hole pair production for incident photon energies ranging from 50 eV to 662 keV for LaBr<sub>3</sub>, CeBr<sub>3</sub>, and CLLB: (a) *e-h* pairs yield as a function of photon energy, and (b) mean energy  $W$  to create an electron-hole pair as a function of incident photon energy.

### C. *Ab initio* calculations for CLLB

In the present study, we performed *ab initio* calculations to determine the essential parameters for thermalization simulations of CLLB, as the basic material properties are not readily available. We employed the Perdew-Burke-Ernzerhof (PBE) [23] exchange-correlation functional and the projector-augmented wave (PAW) method [24] within the framework of density functional theory (DFT), utilizing the Vienna *Ab Initio* Simulation Package (VASP) [25]. A plane-wave basis set with a 520 eV energy cutoff was used for the expansion of electronic wave functions, and spin polarization was activated during calculations. DFT +  $U$  type on-site potentials were included for the La-4*f* ( $U_{\text{eff}} = 10.3$  eV) state, following the work of Åberg *et al.* [26].

CLLB exhibits a cubic elpasolite structure, depicted in Fig. 1, belonging to a large family of quaternary halides with the general formula  $A_2B^I B^{III} X_6$ , where  $A$  and  $B^I$  represent monovalent cations,  $B^{III}$  denotes a trivalent cation, and  $X$  refers to a halogen anion. We relaxed the atomic coordinates until the maximum residual force was below 0.002 eV/Å, yielding a lattice parameter of 11.35 Å, which is in excellent agreement with experimental values. Brillouin zone integration was performed using a  $6 \times 6 \times 6$  Monkhorst-Pack  $k$ -point mesh [27] for a 40-atom unit cell. The results are summarized in Table I.

## III. RESULTS AND DISCUSSION

### A. Intrinsic properties and track structure

Based on a number of simulations at each photon energy, some intrinsic properties of detector materials, such as mean energy required to create an *e-h* pair,  $W$  value, the number of *e-h* pairs, and density of *e-h* pairs can be directly determined from the output of the electron cascade simulations. The number of *e-h* pairs is comparable for LaBr<sub>3</sub>, CeBr<sub>3</sub>, and CLLB, and their electron number distribution determined from the number of events simulated at each incident energy shows an approximately Gaussian profile, exhibiting a similar feature

TABLE II. Simulated electron-hole productions for photon energies ranging from 50 eV to 662 keV, where the mean energy ( $W$ ) to create an electron-hole pair and maximum  $e$ - $h$  pairs yields are compared with the observed light yields. Also,  $SQ$  values are evaluated for LaBr<sub>3</sub>, CeBr<sub>3</sub>, and CLLB.

Materials	$W$ (eV)	$LY_T$ (ph/MeV)	$LY_e$ (ph/MeV)	$SQ$
LaBr <sub>3</sub>	9.5	~105 K	~61–75 K <sup>a,b</sup>	0.71
CeBr <sub>3</sub>	10.7	~92 K	~57–66 K <sup>c</sup>	0.70
CLLB	9.7	~103 K	~50 K <sup>d</sup>	0.44

<sup>a</sup>Reference [28].

<sup>b</sup>Reference [29].

<sup>c</sup>Reference [30].

<sup>d</sup>Reference [31].

to that in other scintillator materials [9,10]. For instance, the average  $e$ - $h$  pairs produced at 10 and 662 keV are 1051 and 69 504, respectively, in LaBr<sub>3</sub>, as compared to 956 and 61 209 in CeBr<sub>3</sub> and 1027 and 68 104 in CLLB. Also, it is interesting to note that the mean  $e$ - $h$  number in these scintillator materials is much higher than in other scintillator materials, such as BaF<sub>2</sub> ( $E_g \sim 10.9$  eV), CaF<sub>2</sub> (11.6 eV) [10], but slightly higher than CsI (5.1 eV) [9], which correlates well with the band gaps of these materials, as expected. Figure 1 shows the electron-hole pair production in LaBr<sub>3</sub>, CeBr<sub>3</sub>, and CLLB as a function of photon energy, where the data points are averaged over  $10^5$  photon simulations for a given energy. The number of  $e$ - $h$  pairs is very similar at low photon energies, but it deviates at higher energies. The number of  $e$ - $h$  pairs created in LaBr<sub>3</sub> is slightly higher than that in CeBr<sub>3</sub>, particularly at higher photon energies, and it is close to that in CLLB. With these  $e$ - $h$  distributions, we can evaluate the  $W$  value, and the results are shown in Fig. 1(b). At energies lower than 1 keV,  $W$  shows a nonlinear behavior and approaches a constant at higher energies for both LaBr<sub>3</sub> and CLLB, while, interestingly, for CeBr<sub>3</sub> as the energy of excitation increases so does  $W$ . Also,  $W$  exhibits sawtooth variations, as observed previously in other detector materials, which is due to the discontinuity at the core-shell edges. While CLLB and LaBr<sub>3</sub> show very similar profile and  $W$  values, the experimental light yield of the former is almost half of the latter. Hence, we can conclude that there is no inherent reason that CLLB cannot increase its light yield and further improve its already good energy resolution. Using the number of  $e$ - $h$  pairs, we can estimate the maximum theoretical light yield achievable for a given scintillator material, which assumes that every  $e$ - $h$  pair eventually recombines to emit a photon [10]. The estimated maximum theoretical light yield,  $LY_T$ , for LaBr<sub>3</sub>, CeBr<sub>3</sub>, and CLLB is given in Table II, along with experimental measurements of light yield for comparison. It is expected that  $LY_T$  values are generally larger than experimental light yields of ~75 000, ~66 000, and ~50 000 for LaBr<sub>3</sub>, CeBr<sub>3</sub>, and CLLB, respectively. In order to explain the discrepancy between experimental light yield and theoretical estimation, Lempicki *et al.* [32] developed a model to calculate the experimental light yield by introducing transfer efficiency  $S$  and luminescence quantum efficiency  $Q$ , which are defined as

$$SQ = LY_e/LY_T, \quad (1)$$

where  $LY_e$  is the measured light yield. The calculated  $SQ$  values for the 662 keV incident photon is also listed in Table II. The  $SQ$  value is very similar for LaBr<sub>3</sub> and CeBr<sub>3</sub>, which is expected because they have a similar electronic structure. In contrast, the  $SQ$  value for CLLB is only 0.44. If we assume high quantum efficiency of Ce<sup>3+</sup> luminescence, it is the energy transfer efficiency that lowers the product, which suggests that nonradiative and quenching processes of thermalization significantly affect the desired recombination of  $e$ - $h$  pairs in CLLB. It is worth noting that a modest 20% increase in the light yield of CLLB from the current 50 000 to 60 000 ph/MeV could lead to improvement in the energy resolution from 3% at 662 keV to 2.7% (following photoelectron statistics). A further increase to 100 000 ph/MeV could lead to a spectacular 2% energy resolution for this material.

To understand how thermalization affects  $e$ - $h$  pair annihilation, the initial spatial distribution of  $e$ - $h$  pairs along ionization tracks needs to be explored because the final light yield is strongly correlated to the density of electronic excitations initially generated along the track regions. This allows us to explore the possible origins of nonlinearity and potential solutions, such as those that utilize codoping effects. The typical spatial distribution of  $e$ - $h$  pairs along ionization tracks for a 10-keV photon interaction is shown in Figs. 2(a)–2(c) for LaBr<sub>3</sub>, CeBr<sub>3</sub>, and CLLB, respectively, where the dimensions in the simulation samples containing all the  $e$ - $h$  pairs are indicated. For example, the interaction of a 10-keV incident photon with a Br atom leads to photoelectric absorption, and spontaneously emits a fast electron with a kinetic energy of 8.446 keV from its  $L_3$  shell (at which the ionization energy is 1.554 keV). As a result, a vacancy (deep hole) is instantaneously created in the same shell, which leads to Br atom excitation to a higher energy state, followed by atomic relaxation to a lower energy state by generating several low-energy electrons. The fast electron slows down through further interactions with atoms to create a large number of  $e$ - $h$  pairs, but with a high density at the end of the tracks. Similar previous studies [9] showed that two major mechanisms, namely interband transitions and plasmon excitation, produce most  $e$ - $h$  pairs observed along the tracks. Interband transitions create electrons with low kinetic energies (a few 10 eV), while the plasmon excitation and decay generate  $e$ - $h$  pairs with their energy lower than the cutoff energy, resulting in these electrons mainly distributed along the tracks. The electrons created by the interband transitions can further create low-energy electrons or interact with phonons, thus leading these electrons to move away from the primary tracks, leaving the holes along the primary tracks. These generation processes of  $e$ - $h$  pairs are consistent with the features of  $e$ - $h$  pair distribution observed in Fig. 2, that is, while the track structures are linearly distributed along fast electron paths, they form high  $e$ - $h$  pair density at the end of the tracks when they slow down. These high-density regions, defined as nanoscale domains of  $e$ - $h$  pairs, are clearly seen in Fig. 2. The simulations show that the spatial distributions of  $e$ - $h$  pairs in LaBr<sub>3</sub> and CeBr<sub>3</sub> are very similar. On the other hand, the number of high-density  $e$ - $h$  domains in CLLB is greater than those in LaBr<sub>3</sub>/CeBr<sub>3</sub>. It is expected that the  $e$ - $h$  pairs in CLLB will be largely decreased during thermalization. This may also lead to a higher level of quenching—considering the much lower light yield of CLLB.

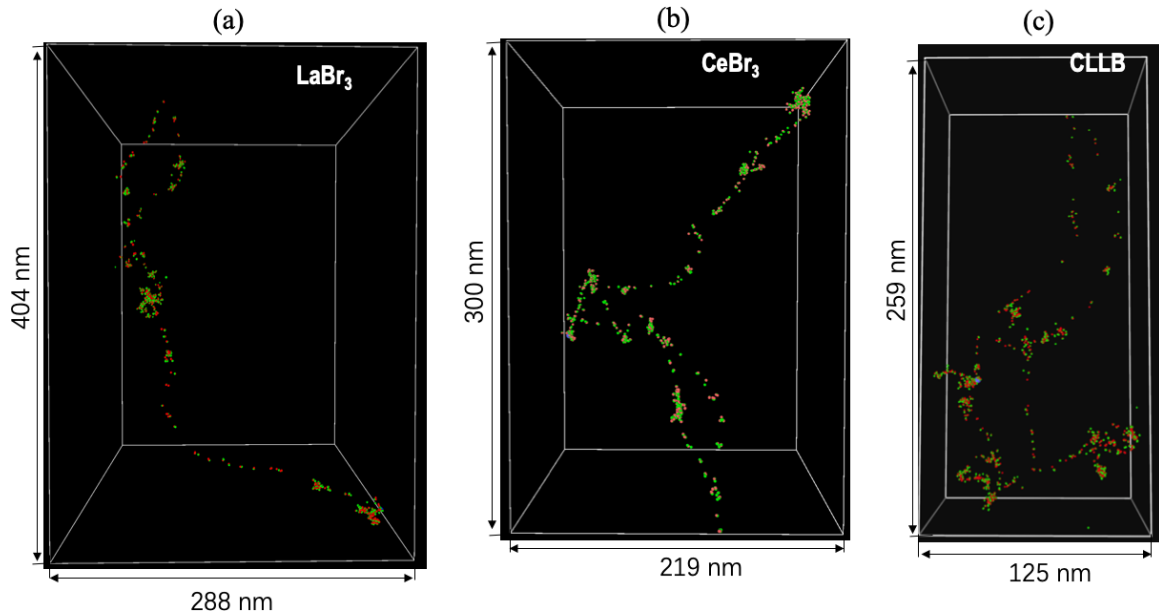


FIG. 2. Simulated spatial distribution of electron-hole pairs for 10-keV photon events in LaBr<sub>3</sub>, CeBr<sub>3</sub>, and CLLB, where green spheres represent electrons and red spheres indicate holes. Due to the large-scale supercells used, the simulation cells show only the regions that contains all the electron-hole pairs created by an incident photon.

We have further analyzed the density of *e-h* pairs in these domains, which is defined as the fraction of the number of *e-h* pairs in a domain to the total number of *e-h* pairs generated for a given photon energy. The results for CLLB are compared only with those in LaBr<sub>3</sub> because the track structures in CeBr<sub>3</sub> are very similar to those in LaBr<sub>3</sub>, as indicated in Figs. 2(a) and 2(b). Figure 3(a) shows the *e-h* pair density in domains for 10-keV photon events in CLLB and LaBr<sub>3</sub> as a function of domain size (from the largest to the smallest) for different cutoff radii of 2 and 8 nm. It is clearly seen that the *e-h* pair density in CLLB is generally higher than that in LaBr<sub>3</sub>, which slightly depends on the cutoff, and decreases with decreasing

domain size. Some large *e-h* pair domains can be formed in CLLB with the *e-h* pair density greater than 30% of the total *e-h* pairs created. The *e-h* pair density in the largest *e-h* domains for the cutoff radii of 2, 5, and 8 nm is exhibited in Fig. 3(b). Except for 2-nm cases, the *e-h* pair density in the largest domains in CLLB is generally higher than that in LaBr<sub>3</sub>, particularly for the cutoff of 8 nm in which the *e-h* pair density is almost doubled. The high *e-h* pair density produced in CLLB, along with the number of high-density *e-h* domains, leads to a large decrease in the *e-h* pairs during the thermalization, resulting in a much lower light yield of CLLB as observed in experimental measurements.

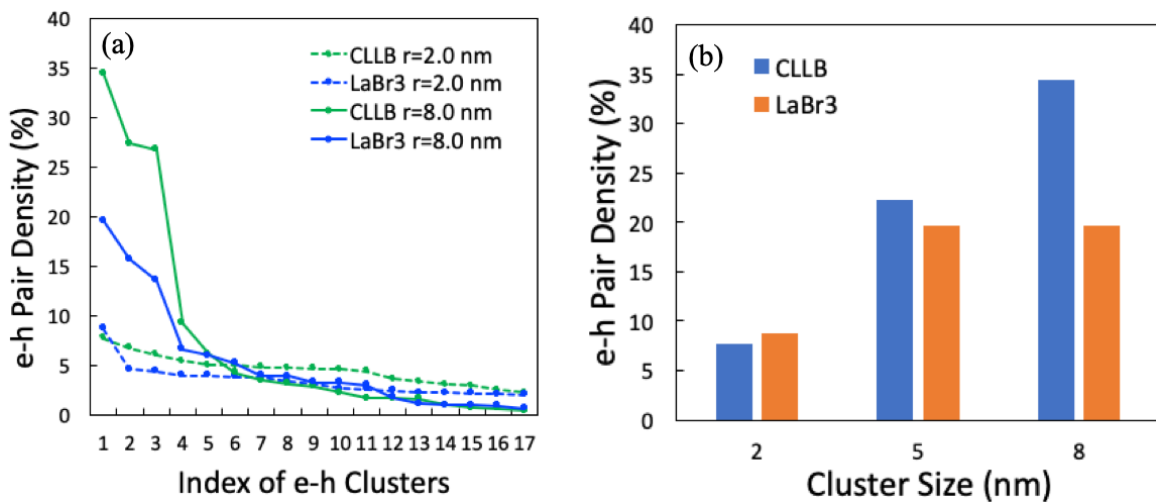


FIG. 3. Cluster distribution and the density of *e-h* pairs in domains for 10-keV photon events in CLLB and LaBr<sub>3</sub>: (a) *e-h* pair density as a function of *e-h* domain index, where the smaller index indicates the large size *e-h* domain for two different cutoff radii, and (b) *e-h* density of the largest domains for the cutoff radii of 2 and 8 nm.

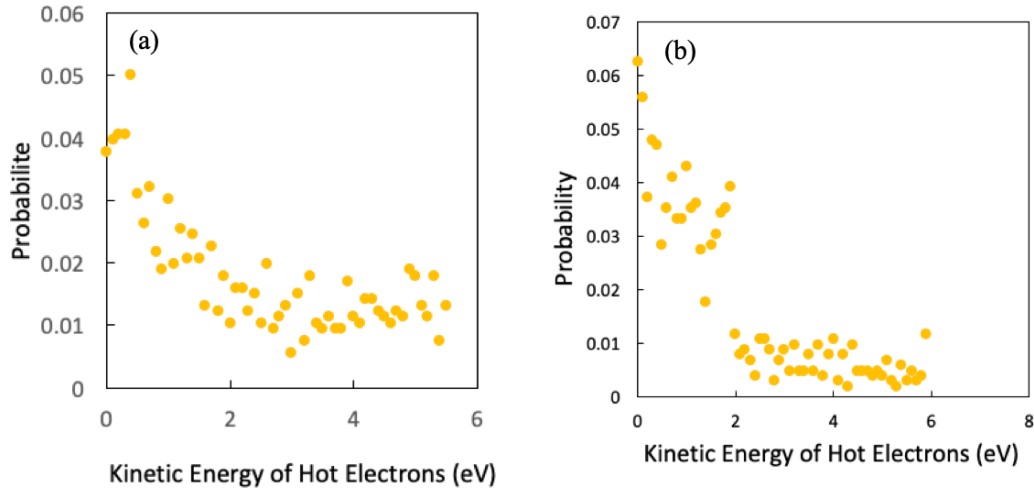


FIG. 4. The distribution probability of kinetic energy of hot electrons, as simulated by NWEGRIM code: (a) in  $\text{LaBr}_3$ , and (b) in CLLB, where a binomial distribution is apparent.

### B. Thermalization of $e$ - $h$ pairs

As described above, the spatial distribution of  $e$ - $h$  pairs and electronic structure of  $\text{CeBr}_3$  are very similar to those of  $\text{LaBr}_3$ , but are different for CLLB. Therefore, the thermalization simulation will focus on  $\text{LaBr}_3$  and CLLB so that a better comparison can be made. In addition to the track structures and  $e$ - $h$  distributions, the kinetic energies of electrons at the end of electron cascades provide the initial energy distributions for thermalization simulations of  $e$ - $h$  pairs. Based on the  $e$ - $h$  pair production simulated by the NWEGRIM code, we further analyzed the distribution in the energy of hot electrons in  $\text{LaBr}_3$  and CLLB, and the results are shown in Fig. 4. There seems to be a transition at around 1.9 eV, which may be attributed to the low-level core-shell ionization of Li. Based on the spatial and energy distributions of  $e$ - $h$  pairs, along with the basic materials properties as inputs (see Table I), we have modeled the thermalization of hot electrons in both materials. Figures 5(a) and 5(b) show the initial  $e$ - $h$  distributions along the ionization tracks for  $\text{LaBr}_3$  and CLLB, respectively, whereas Figs. 5(c) and 5(d) show them after thermalization for a 10-keV photon, where the dimensions are indicated at different scales. In these simulations, the holes are assumed to be static or instantaneously self-trapped, and thus the track structures of holes (red dots) are very similar to those before thermalization. However, it should be noted that the number of holes in these tracks is reduced due to the (nonradiative) recombination of  $e$ - $h$  pairs during thermalization. The large difference appears in the spatial distribution of electrons, which can be clearly seen in Figs. 5(c) and 5(d), and a number of electrons generally diffuse away from the initial ionization track. However, the density of excitation in  $\text{LaBr}_3$  is much higher and in CLLB seems slightly diffuse. This may lead to steeper gradients in  $\text{LaBr}_3$ , resulting in varying density effects and worse proportionality (nonlinearity), which is a composite of all effects. The fraction of recombined electrons with holes in  $\text{LaBr}_3$  is about 30% at all energies, while it is about 45% in CLLB. The current study considers the internal electric field (IEF), which leads to the attraction of electrons and holes, and may enhance electron recombination. The smaller the

dielectric constant is, the stronger the IEF [8]. As shown in Table I, the static dielectric constant is very similar for both materials, which suggests that the IEF has a similar effect on  $e$ - $h$  recombination. As discussed above, both the larger number and higher density of  $e$ - $h$  domains in CLLB lead to strongly attractive electron-hole interactions, resulting in a greater fraction of recombined (lost) electrons. The greater number and higher density of  $e$ - $h$  domains affect the electron thermalization process in two immediate ways: (a) the fraction of recombined electrons is increased, and (b) repulsive electron-electron interactions lead to longer thermalization distances, thus more diffused spatial distribution. On the other hand, the electron effective mass in CLLB is much larger than that in  $\text{LaBr}_3$ , as shown in Table I. A large electron effective mass decreases the mean free path of electrons after electron-phonon interaction, thus preventing the electrons from traveling further away from the initial track of immobile self-trapped holes and enhancing the local recombination of  $e$ - $h$  pairs. Another important factor that affects the thermalized track structure is LO phonon energy: A large LO phonon energy increases the probability for electrons to slow down quickly, which inhibits electrons from moving away from the initial track and also recombination. The slightly high energies of both LO and A phonons in  $\text{LaBr}_3$ , as compared to those in CLLB, may also account for the higher density of excitation close to the initial track observed in  $\text{LaBr}_3$ . Based on all these factors, we can conclude that the local high  $e$ - $h$  pair density and a large number of high-density  $e$ - $h$  domains created in CLLB are the major factors affecting the recombination of  $e$ - $h$  pairs during thermalization. The present investigation further verifies our hypothesis that the  $e$ - $h$  pair density along the ionization track, high-density domains, and their variation with incident photon energy represent one of the key competing processes responsible for the generation of light yield and nonlinearity in scintillator materials.

Figure 6 summarizes the number of  $e$ - $h$  pairs as a function of photon energy before and after thermalization in  $\text{LaBr}_3$  and CLLB. Our previous study demonstrated that the LO phonon energy is found to be the major parameter determining

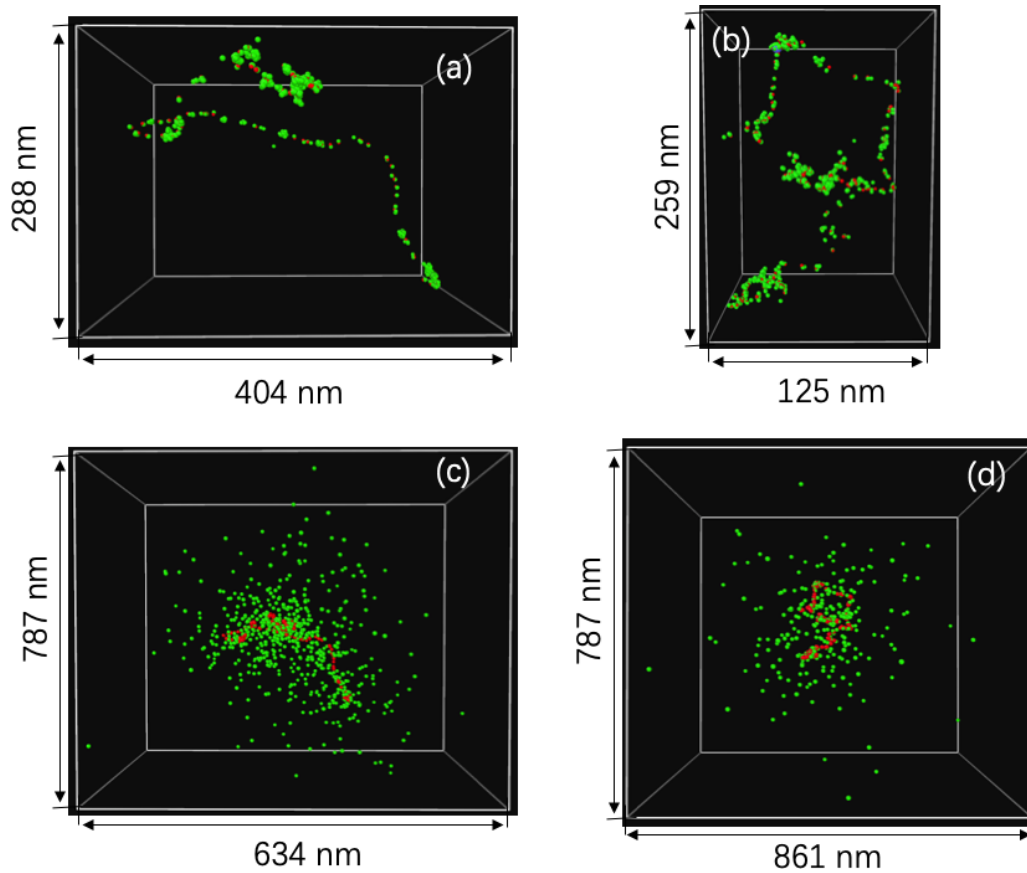


FIG. 5. Simulated spatial distribution of  $e-h$  pairs created by 10-keV photons in LaBr<sub>3</sub> (a) and CLLB (b) before thermalization, and (c) and (d) after thermalization, respectively. Green spheres represent electrons and red spheres indicate holes. Comparison of thermalized  $e-h$  pair distributions clearly demonstrates that the density of excitation in LaBr<sub>3</sub> is much higher and in CLLB it seems more diffuse. Similar to Fig. 2, the simulation cells show only the regions that contains all the electron-hole pairs created by an incident photon and thermalized electrons.

the differences in thermalization time and distance between two materials [7], but the extent of  $e-h$  pair recombination is found to vary among the two materials. The electron mean free path, LO phonon energy, and static dielectric constant are identified as the principal factors responsible for these variations. As described above, the initial  $e-h$  pair density

plays a significant role in the recombination of  $e-h$  pairs. The initial number of  $e-h$  pairs (before thermalization) in CLLB is close to that in LaBr<sub>3</sub> because of very similar  $W$  values, as shown in Table II. However, the number of  $e-h$  pairs in CLLB is smaller than that in LaBr<sub>3</sub> after thermalization, which may be associated with the number of high-density  $e-h$  domains

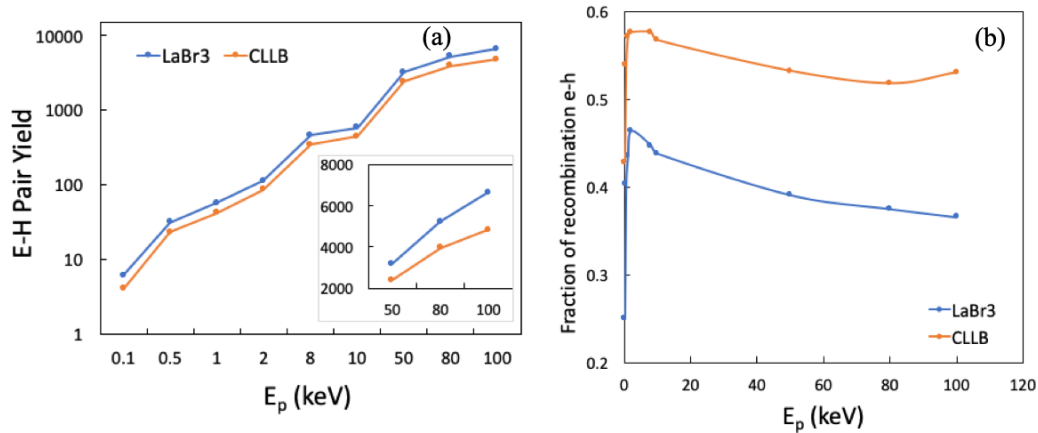


FIG. 6. (a) Comparison of the number of  $e-h$  pairs before and after thermalization in LaBr<sub>3</sub> and CLLB, where the yield in inset clearly indicates the difference at high incident photon energies, and (b) the recombination fraction of  $e-h$  pairs after thermalization as a function of photon energy.

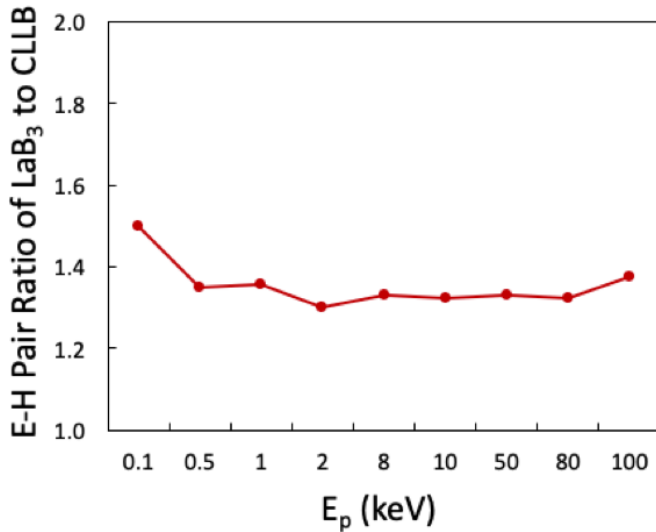


FIG. 7. The  $e$ - $h$  pair ratio of LaBr<sub>3</sub> to CLLB as a function of photon energy. Note that the ratio is close to the ratio of LY experimental values ( $\sim 1.5$ , see Table II).

in CLLB, thus giving rise to the significant reduction of  $e$ - $h$  pairs for all the photon energies studied. Figure 6(b) shows the fraction of electron recombination during thermalization. For the photon energies lower than 1 keV, the recombination fraction is small because only a few  $e$ - $h$  pairs are created and the high-density domains along the tracks are hardly established. For example, the incident photons with 100 eV create, on average, only eight and seven  $e$ - $h$  pairs for LaBr<sub>3</sub> and CLLB, respectively. However, when the photon energy is larger than 1 keV, the recombination fraction decreases with increasing incident photon energy, which may be attributed to the increased stopping power at relatively low incident energies (1–2 keV), thus generating high  $e$ - $h$  pair density and increasing the probability for  $e$ - $h$  pair recombination. To better understand the probability of  $e$ - $h$  pair recombination in these two materials, the ratio of the survived  $e$ - $h$  pairs in LaBr<sub>3</sub> to CLLB is shown in Fig. 7, which is calculated based on the data in Fig. 6(a). It is interesting to note that the average ratio is almost constant and is between 1.35 and 1.4. Experimentally, the measured light yield is 75 000 and 50 000 for LaBr<sub>3</sub> and CLLB, respectively, which results in the ratio of 1.5. The calculated ratio from thermalization is close to the ratio of measured light yields for these two materials. This demonstrates that the thermal quenching is important for the final light yield of CLLB observed in experiments.

#### IV. CONCLUSIONS

The Monte Carlo approach of thermalization has been applied to study the  $e$ - $h$  recombination and the different processes controlling the thermalization in LaBr<sub>3</sub> and CLLB. The initial  $e$ - $h$  pairs and their ionization track structures are simu-

lated using the NWEGRIM code that considers various energy loss mechanisms to slow down charge carriers. In simulated materials, the number of  $e$ - $h$  pairs almost linearly increases with increasing incident photon energy with the highest and lowest numbers in LaBr<sub>3</sub> and CeBr<sub>3</sub>, respectively, which is consistent with  $W$  values determined for these scintillators.  $W$  values vary at low incident photon energies, but approach a constant for LaBr<sub>3</sub> and CLLB at higher energies, as expected.

Using NWEGRIM, we generated the ionization tracks, which show that the density of  $e$ - $h$  pairs and high  $e$ - $h$  pair density domains are very similar in LaBr<sub>3</sub> and CeBr<sub>3</sub>, even though the production of  $e$ - $h$  pairs is slightly different. In contrast, the number of high-density domains and the  $e$ - $h$  pair density along the ionization tracks in CLLB are higher. Considering that the thermalization is strongly correlated to the ionization track structures, rather than the number of  $e$ - $h$  pairs, the thermalization simulation focused on LaBr<sub>3</sub> and CLLB so that a better comparison can be made.

The thermalization of  $e$ - $h$  pairs in LaBr<sub>3</sub> and CLLB shows a clear variation in ionization tracks. The local density of  $e$ - $h$  pairs in LaBr<sub>3</sub> appears to be much higher than that in CLLB, but their spatial distribution seems more diffuse in CLLB. It is of interest to note that the high-density domains disappear after thermalization in both materials, which may be attributed to local electron annihilation with holes and electrons diffusing away. The electron effective mass, LO phonon energy, and dielectric constant all play important roles in the thermalization process, thus affecting the spatial distribution of  $e$ - $h$  pairs. The results demonstrate that the initial  $e$ - $h$  pair density along the ionization track, high-density domains, and their variation with incident photon energy are the key factors attributing to thermalization and responding to the generation of light yield and nonlinearity in scintillator materials.

The results also explain the varying experimental properties of studied materials. They support the presence of higher light yield and nonproportionality in LaBr<sub>3</sub>, slightly lower light yield and worse energy resolution in CeBr<sub>3</sub>, and finally, lower light yield and good energy resolution in CLLB. The methodology presented in this paper can be used to evaluate other materials for their theoretical light yield, nonproportionality, and potential energy resolution. It can support the development of new and improvement of existing materials by providing guidance on materials engineering. For example, it has already been shown that codoping, which interferes with the density effects, can lead to a reduction in the nonproportionality and improvements in energy resolution [33,34].

#### ACKNOWLEDGMENTS

This research was supported by the U.S. Defense Threat Reduction Agency (DTRA, Award No. HDTRA1-20-2-0002), Interaction of Ionizing Radiation with Matter (IIRM), and University Research Alliance (URA). The DFT computations involved in this work were conducted on the Frontera cluster of the Texas Advanced Computing Center.

[1] P. Dorenbos, M. Marsman, and C. W. E. Van Eijk, in *Proceedings of the International Conference on Inorganic Scintillators*

*and their Applications* (Delft University Press, The Netherlands, 1996), pp. 148–155.

- [2] G. Bizarri *et al.*, *Phys. Status Solidi C* **6**, 97 (2009).
- [3] G. Bizarri *et al.*, *J. Appl. Phys.* **105**, 044507 (2009).
- [4] G. Bizarri *et al.*, *J. Lumin.* **129**, 1790 (2009).
- [5] S. Payne *et al.*, *IEEE Trans. Nucl. Sci.* **NS-56**, 2506 (2009).
- [6] R. T. Williams, J. Q. Grim, Q. Li, K. B. Ucer, and W. W. Moses, *Phys. Status Solidi B* **248**, 426 (2011).
- [7] Z. G. Wang, Y. L. Xie, B. D. Cannon, L. W. Campbell, F. Gao, and S. Kerisit, *J. Appl. Phys.* **110**, 064903 (2011).
- [8] Z. G. Wang, Y. L. Xie, L. W. Campbell, F. Gao, and S. Kerisit, *J. Appl. Phys.* **112**, 014906 (2012).
- [9] F. Gao, Y. Xie, S. Kerisit, L. W. Campbell, and W. J. Weber, *Nucl. Instrum. Methods Phys. Res. A* **652**, 564 (2011).
- [10] F. Gao, Y. L. Xie, Z. G. Wang, S. Kerisit, D. X. Wu, L. W. Campbell, R. M. Van Ginhoven, and M. Prange, *J. Appl. Phys.* **114**, 173512 (2013).
- [11] A. Syntfeld, R. Arlt, V. Gostilo, A. Loupilov, M. Moszyński, A. Nassalski, M. Swoboda, and D. Wolski, *IEEE Trans. Nucl. Sci.* **53**, 3938 (2006).
- [12] P. Guss, M. Reed, D. Yuan, A. Reed, and S. Mukhopadhyay, *Nucl. Instrum. Methods Phys. Res. A* **608**, 297 (2009).
- [13] D. E. Cullen, J. H. Hubbell, and L. Kissel, EPDL97 The Evaluated Data Library, 97 version, Report No. UCRL-50400, 1997, Vol. 6, Rev. 5.
- [14] J. Llacer and E. L. Garwin, *J. Appl. Phys.* **40**, 2766 (1969).
- [15] M. Sparks, D. L. Mills, R. Warren, T. Holstein, A. A. Maradudin, L. J. Sham, E. Loh Jr., and D. F. King, *Phys. Rev. B* **24**, 3519 (1981).
- [16] J. N. Bradford and S. Woolf, *J. Appl. Phys.* **70**, 490 (1991).
- [17] B. Liu, M. Gu, Z. M. Qi, X. L. Liu, S. M. Huang, and C. Ni, *Phys. Rev. B* **76**, 064307 (2007).
- [18] X. Gao and Y. J. He, *J. Chin. Ceram. Soc.* **38**, 878 (2010).
- [19] W. Setyawan, R. M. Gaume, R. S. Feigelson, and S. Curtarolo, *IEEE Trans. Nucl. Sci.* **56**, 2989 (2009).
- [20] M. Loyd *et al.*, *J. Cryst. Growth* **531**, 125365 (2020).
- [21] The Materials Project: <https://materialsproject.org/materials/mp-569850>.
- [22] B. Wu *et al.*, *J. Am. Ceram. Soc.* **104**, 1489 (2021).
- [23] J. P. Perdew, K. Burke, and M. Ernzerhof, *Phys. Rev. Lett.* **77**, 3865 (1996).
- [24] P. E. Blöchl, *Phys. Rev. B* **50**, 17953 (1994).
- [25] G. Kresse and J. Furthmüller, *Phys. Rev. B* **54**, 11169 (1996).
- [26] D. Åberg, B. Sadigh, A. Schleife, and P. Erhart, *Appl. Phys. Lett.* **104**, 211908 (2014).
- [27] H. J. Monkhorst and J. D. Pack, *Phys. Rev. B* **13**, 5188 (1976).
- [28] E. V. D. van Loef, P. Dorenbos, C. W. E. van Eijk, K. Krämer, and H. U. Güdel, *Appl. Phys. Lett.* **79**, 1573 (2001).
- [29] M. Moszyński, Ł. Świdorski, T. Szcześniak, A. Nassalski, A. Syntfeld-Każuch, W. Czarnacki, G. Pausch, J. Stein, P. Lavoute, F. Lherbert, and F. Kniest, *IEEE Trans. Nucl. Sci.* **55**, 1774 (2008).
- [30] F. G. A. Quarati, P. Dorenbos, J. van der Biezen, A. Owens, M. Selle, L. Parthier, and P. Schotanus, *Nucl. Instrum. Methods Phys. Res. A* **729**, 596 (2013).
- [31] U. Shirwadkar *et al.*, *Nucl. Instrum. Methods Phys. Res. A* **652**, 268 (2011).
- [32] A. Lempicki and A. J. Wojtowicz, *J. Lumin.* **60-61**, 942 (1994).
- [33] M. S. Alekhin, J. T. M. de Haas, I. V. Khodyuk, K. W. Krämer, P. R. Menge, V. Ouspenski, and P. Dorenbos, *Appl. Phys. Lett.* **102**, 161915 (2013).
- [34] F. G. A. Quarati, M. S. Alekhin, K. W. Krämer, and P. Dorenbos, *Nucl. Instrum. Methods Phys. Res. A* **735**, 655 (2014).